

Zeolitic Imidazolate Framework-Derived Core-Shell-Structured $\text{CoS}_2/\text{CoS}_2\text{-N-C}$ Supported on Electrochemically Exfoliated Graphene Foil for Efficient Oxygen Evolution

Junhui Cao,^[a] Chaojun Lei,^[a] Bin Yang,^[a] Zhongjian Li,^[a] Lecheng Lei,^[a] Yang Hou,^{*[a]} and Xinliang Feng^[b]

Developing earth-abundant transition-metal based materials to efficiently catalyze the oxygen evolution reaction (OER) is an urgent demand for electrochemical water splitting and rechargeable metal-air batteries. Here, we developed a novel 3D hybrid electrocatalyst consisting of core-shell structured $\text{CoS}_2/\text{CoS}_2$ embedded into N-doped carbon supported on electrochemically exfoliated graphene foil ($\text{EG}/\text{CoS}_2/\text{CoS}_2\text{-NC}$) by sulfurization treatment of $\text{EG}/\text{Co(OH)}_2$ /zeolitic imidazolate framework-67 (ZIF-67) as precursor. The thickness of the $\text{CoS}_2\text{-NC}$ shell derived from ZIF-67 is 10 nm and the CoS_2 core generated from Co(OH)_2 nanosheet arrays has a particle size of ~20 nm. Benefiting from the unique 3D core-shell structure and synergistic effects, the $\text{EG}/\text{CoS}_2/\text{CoS}_2\text{-NC}$ hybrid enormously promotes electrocatalytic OER activity with a low overpotential of 210 mV at a current density of 10 mA cm^{-2} and a small Tafel slope of 61.9 mV dec^{-1} . These values are far superior compared to the commercial Ir/C catalyst, and even better than other reported state-of-the-art CoS_2 -based materials. In-situ Raman spectroscopy together with ex-situ XRD patterns reveal that the active centers of $\text{EG}/\text{CoS}_2/\text{CoS}_2\text{-NC}$ hybrid are proven to be Co-OOH species that are derived from Co-S groups during the OER process. The superb catalytic performance is also reflected in boosting electrochemical urea oxidation and hydrazine oxidation, where the accelerated oxidation reaction could be observed.

Rechargeable metal-air batteries and water electrolyzers have been proved to be promising technologies for effective conversion of renewable energy to alleviate the rapidly increased energy demands.^[1] Both two half reactions of oxygen

evolution reaction (OER) and oxygen reduction reaction (ORR) in metal-air batteries as well as OER and hydrogen evolution reaction in water electrolyzers require a considerably high OER performance to drive overall energy conversion process efficiently. However, a sluggish four-electron transfer process severely hinders the OER kinetics, leading to a poor OER activity.^[2] Designing and developing high performance electrocatalysts to accelerate the OER process is crucial towards the development of clean rechargeable metal-air batteries and water splitting systems.^[3] Thus far, noble-metal based electrocatalysts (e.g., IrO_2 -based,^[4] RuO_2 -based^[5]) are the most efficient electrocatalyst towards OER in alkaline media. However, the considerable expense and scarcity in storage largely limits their practical applications, thus the widespread applications of metal-air batteries and water electrolyzers in commerce are further hindered.^[5] Consequently, it is imperative to develop non-precious metal based materials to replace the precious metal catalysts to meet the large-scale application of these renewable energy conversion technologies.^[6]

As a conventional transition metal sulfide, cobalt disulfide proves itself to be an excellent electrocatalyst owing to its low cost and outstanding catalytic performance towards OER.^[7] Despite certain accomplishments, single-component cobalt sulfide is commonly in ordinary performance with poor stability. Also, the mechanism of how cobalt sulfide could catalyze OER yet has not been thoroughly studied. Combining the cobalt sulfide with nanocarbon seems to be an inspiring strategy to achieve better overall electrocatalytic performance with different functions for synergistic enhancement.^[1e,8] Among various nanocarbon materials, the N-doped nanocarbon exhibits excellent conductivity, superior electron structure, and impressive electrocatalytic performance^[9] and has been considered as one of the most promising choice.

Herein, we developed a novel 3D hybrid electrocatalyst with a core-shell structured $\text{CoS}_2/\text{CoS}_2$ embedded into N-doped carbon grown on electrochemically exfoliated graphene foil ($\text{EG}/\text{CoS}_2/\text{CoS}_2\text{-NC}$) prepared by a vapor-phase hydrothermal growth of ZIF-67 on the surface of $\text{EG}/\text{Co(OH)}_2$ nanosheets array, followed by a vacuum sulfurization strategy. In this $\text{EG}/\text{CoS}_2/\text{CoS}_2\text{-NC}$ hybrid, the core part is composed of Co(OH)_2 nanosheets array-derived CoS_2 with ~20 nm particle size, and the shell part is $\text{CoS}_2\text{-NC}$ with 10 nm thickness derived from ZIF-67 precursor. The unique 3D core-shell structure and synergistic effect of $\text{EG}/\text{CoS}_2/\text{CoS}_2\text{-NC}$ hybrid contribute to an impressive

[a] J. Cao, C. Lei, Prof. B. Yang, Prof. Z. Li, Prof. L. Lei, Prof. Y. Hou
Key Laboratory of Biomass Chemical Engineering of Ministry of Education
College of Chemical and Biological Engineering
Zhejiang University
Hangzhou, China
E-mail: yhou@zju.edu.cn

[b] Prof. X. Feng
Department of Chemistry and Food Chemistry
Center for Advancing Electronics Dresden (CFAED)
Technische Universität Dresden
01062 Dresden, Germany.

 Supporting information for this article is available on the WWW under
<https://doi.org/10.1002/batt.201800098>

 An invited contribution to a Special Issue on Bifunctional Catalysts for Metal-Air Batteries

OER performance, featured by a low overpotential of 210 mV at 10 mA cm^{-2} and a small Tafel slope of 61.9 mV dec^{-1} . Such a superior OER activity is far higher than that of the commercial Ir/C catalyst, and well comparable to previously reported state-of-the-art CoS₂-based materials. The in-situ Raman spectra combined with ex-situ XRD patterns, reveal that the active sites in EG/CoS₂/CoS₂-NC hybrid are Co-OOH species derived from Co-S groups, which could efficiently boost the OER process. Furthermore, the EG/CoS₂/CoS₂-NC hybrid exhibits the highest electrocatalytic activity towards both urea oxidation and hydrazine oxidation reactions by exhibiting the largest current density at the given voltage range and the smallest Tafel slopes of 262 and 89.7 mV dec^{-1} , compared with other control electrodes.

The procedure to fabricate EG/CoS₂/CoS₂-NC hybrid is illustrated in Scheme 1. The Co(OH)₂ nanosheets array was first electrochemically deposited on the surface of EG foil that was produced by electrochemical exfoliation treatment of graphite foil. The ZIF-67 precursor was subsequently introduced to the surface of as-prepared EG/Co(OH)₂ by a vapor-phase hydrothermal growth strategy. The final EG/CoS₂/CoS₂-NC hybrid could be obtained by further sulfurization treatment of EG/Co(OH)₂/ZIF-67. The synthesis details are shown in the Supporting Information. After a systematical study on the influence of sulfurization temperature (Figure S1), the optimal temperature was found to be 400°C . Therefore, all EG/CoS₂/CoS₂-NCs denoted in this work refer to the EG/CoS₂/CoS₂-NC sample sulfurized under 400°C , unless pointed out otherwise.

Figure 1a-1b show the field-emission scanning electron microscopy (FESEM) images of EG/Co(OH)₂/ZIF-67 and EG/CoS₂/CoS₂-NC. It can be clearly observed that the EG/Co(OH)₂/ZIF-67 nanosheets possessed a vertically-oriented layered structure with a thickness of about 30 nm. After the sulfurization treatment of EG/Co(OH)₂/ZIF-67 under 400°C , the original nanosheet array structure was not obviously destroyed, but new nanoparticle-piled array structure was formed (Figure 1b). Such a change in morphology can be attributed to the successful conversion of the nanosheets array of EG/Co(OH)₂/ZIF-67 to gathered nanoparticles array of EG/CoS₂/CoS₂-NC.^[10] Transmission electron microscopy (TEM) was utilized to further investigate the microstructure of EG/CoS₂/CoS₂-NC. Figure 1c

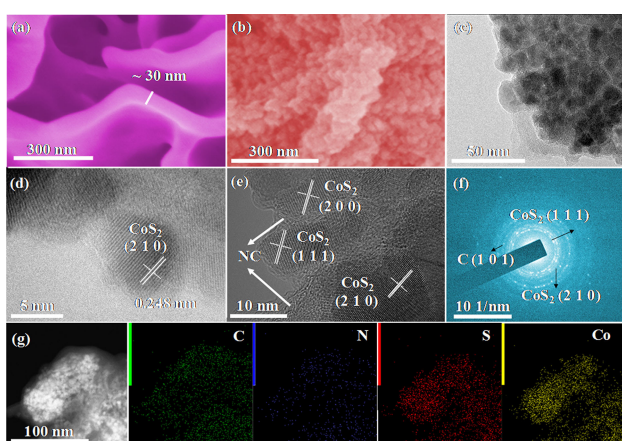
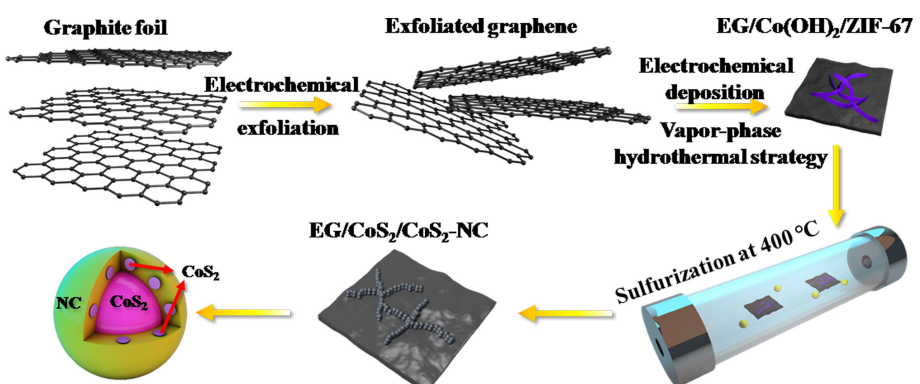


Figure 1. a)-b) FESEM images of EG/Co(OH)₂/ZIF-67 and EG/CoS₂/CoS₂-NC, c) TEM image of EG/CoS₂/CoS₂-NC, d)-e) HRTEM images of EG/CoS₂/CoS₂-NC, f) SAED pattern of EG/CoS₂/CoS₂-NC, g) EDX images of EG/CoS₂/CoS₂-NC.

shows a low-magnification TEM image of EG/CoS₂/CoS₂-NC, from which the CoS₂ core with a particle size of $\sim 20 \text{ nm}$ could be clearly seen. The edge of EG/CoS₂/CoS₂-NC was mainly composed of $\sim 10 \text{ nm}$ -thick CoS₂-NC shells, as a result of the sulfurization of ZIF-67. The high-resolution TEM (HRTEM) images of EG/CoS₂/CoS₂-NC showed that in the CoS₂-NC shell, the CoS₂ was well embedded into the $1 \sim 2 \text{ nm}$ thick amorphous carbon layers (Figure 1d-1e). An interplanar distance of 0.248 nm could be indexed to the (210) plane of CoS₂ (Figure 1d). Besides the CoS₂-NC derived from outer ZIF-67 shell, the CoS₂ core derived from Co(OH)₂ nanosheets array was also observed in the inside of EG/CoS₂/CoS₂-NC hybrid. The lattice fringe spacings of 1.97 nm , 3.21 nm , and 0.249 nm corresponding to the (200), (111) and (210) planes of CoS₂ could be found in Figure 1e. Furthermore, the diffraction rings of selected area electron diffraction (SAED) pattern shown in Figure 1f further confirmed that the EG/CoS₂/CoS₂-NC hybrid was composed of CoS₂ and carbon based on the (111) and (210) planes of CoS₂ and (101) plane of graphite, respectively. In contrast, the TEM images of EG/CoS₂ and EG/CoS₂-NC are provided in Figure S2-S3. It is notable that the nanocarbon shells could not be formed in the EG/CoS₂, indicating that the N-doped carbon was derived from



Scheme 1. Fabrication process for the EG/CoS₂/CoS₂-NC hybrid.

ZIF-67. Energy dispersive X-ray spectrum (EDX) and elemental mapping was conducted to examine the element composition and distribution in Figure 1g. The C, S, and Co elements were detected with high intensities, while N element was identified with a low intensity, which implies that the N atoms was successfully doped into the carbon shells forming N-doped carbon, as a result of thermal treatment of ZIF-67.

The X-ray diffraction (XRD) pattern of EG/CoS₂/CoS₂-NC is displayed as Figure 2a, where the diffraction peak located at 27.5° belongs to (002) face of carbon, and other diffraction peaks located at 28.0°, 32.4°, and 36.3° could be indexed to (111), (200), and (210) faces of CoS₂ (JPDF 41-1471),^[9a,11] respectively. These peaks further evidence the coexistence of CoS₂ and N-doped carbon in the EG/CoS₂/CoS₂-NC hybrid. In Figure 2b, the D band at 1364 cm⁻¹ and G band at 1545 cm⁻¹ could be detected in the Raman spectrum of EG/CoS₂/CoS₂-NC. The I_D/I_G ratio is about 0.91, indicating the N-doping created defects in the carbon shells of EG/CoS₂/CoS₂-NC. X-ray photoelectron spectroscopy (XPS) was used to confirm the chemical states of elements in the EG/CoS₂/CoS₂-NC hybrid. Broad XPS result shown in Figure S4 reveals the presence of C, N, S, and Co elements. Deconvolution into the high-resolution Co 2p XPS displays the existence of Co 2p peaks located at 782.5 and 785.7 eV, indexed to the Co²⁺ 2p_{3/2} and Co³⁺ 2p_{3/2} peaks (Figure 2c), respectively,^[12] which agrees well with previously reported Co 2p XPS of CoS₂.^[13] Two doublets could be observed in the high-resolution S 2p XPS spectrum of EG/CoS₂/CoS₂-NC (Figure 2d). The first pair located at 163.3 and 164.5 eV belongs to the Co–S bonds of CoS₂,^[7a,13] while the other one located at 168.9 and 169.9 eV is considered to be donated by the absorption of oxygen with sulfur on the surface.^[7b,14] The high-resolution N 1s XPS spectrum of EG/CoS₂/CoS₂-NC further

confirms the N-doping into the nanocarbon shell, featured by the graphitic N at 402.0 eV, pyrrolic N at 400.9 eV, and pyridine N at 399.9 eV (Figure 2e).^[15] The appearance of C–N and C=N bonds is further supported in the high-resolution C 1s XPS result (Figure 2f).^[16] The contact wetting angle of the EG/CoS₂/CoS₂-NC is measured to be 24.5° (Figure S5), indicating a hydrophilic nature, which could enhance the ion trapping process, thus making the OER process more facile.

The EG/CoS₂/CoS₂-NC hybrid was directly utilized as the electrode, and the electrocatalytic performance towards OER was evaluated in 1.0 M KOH with a conventional three-electrode system. All potentials are converted to the reversible hydrogen electrode (RHE). Figure 3a shows the *iR*-corrected polarization curves of EG/CoS₂, EG/CoS₂-NC, EG/CoS₂/CoS₂-NC, and Ir/C electrocatalysts. Among the four electrodes, the EG/CoS₂/CoS₂-NC hybrid exhibits the best catalytic performance towards OER with the lowest overpotential of 210 mV at the current density of 10 mA cm⁻², while the overpotentials of EG/CoS₂ and EG/CoS₂-NC are 292 and 335 mV, respectively. The superior catalytic activity of EG/CoS₂/CoS₂-NC overwhelms that of EG/CoS₂ and EG/CoS₂-NC, indicating that the synergistic effect between CoS₂ and CoS₂-NC play key role in OER process. The performance of commercial Ir/C to catalyze OER was also tested, but the OER activity falls behind that of EG/CoS₂/CoS₂-NC significantly, with a high overpotential of 312 mV at 10 mA cm⁻². Furthermore, the current densities at the overpotential of 300 mV were compared for all samples. The largest current density of 35.3 mA cm⁻² belongs to the EG/CoS₂/CoS₂-NC, which is even larger than the sum of EG/CoS₂ (13.9 mA cm⁻²) and EG/CoS₂-NC (6.49 mA cm⁻²), as well as the current density of commercial Ir/C (8.67 mA cm⁻²). The overpotentials of four electrocatalysts working at 50 mA cm⁻² was

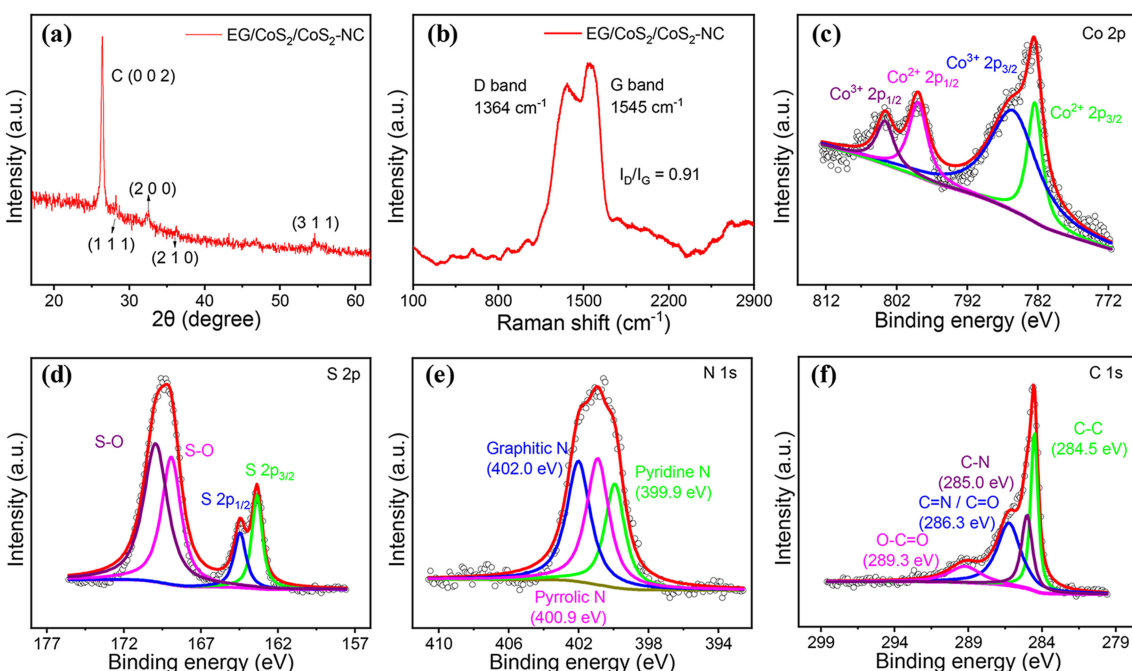


Figure 2. a)-b) XRD pattern and Raman spectrum of EG/CoS₂/CoS₂-NC, c)-f) High-resolution Co 2p, S 2p, N 1s and C 1s XPS of EG/CoS₂/CoS₂-NC.

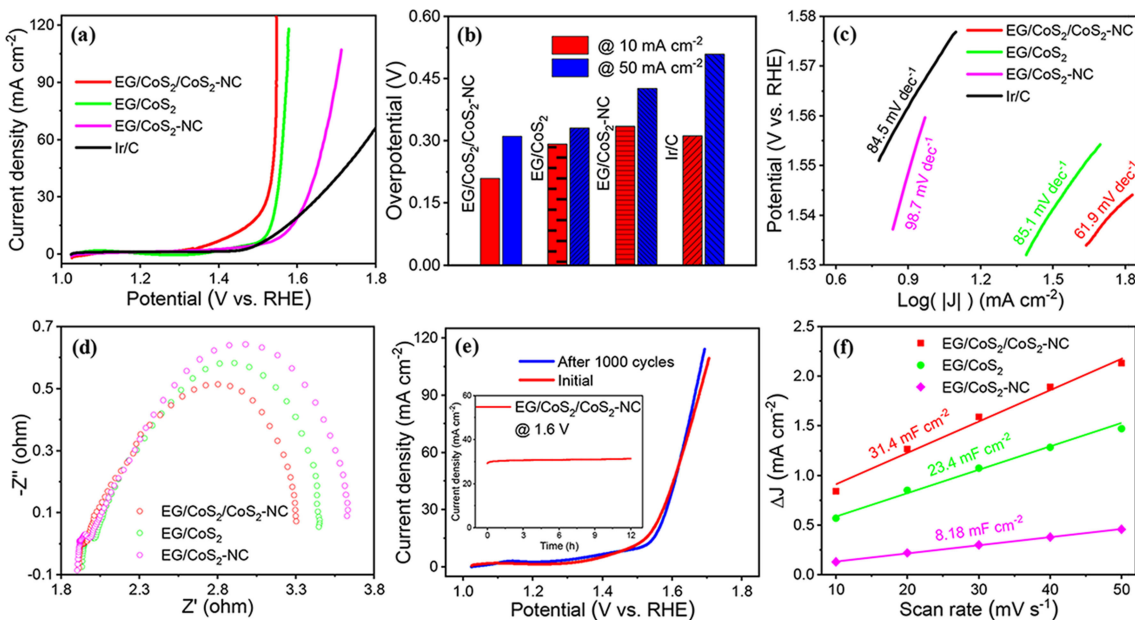


Figure 3. a) Polarization curves of EG/CoS₂, EG/CoS₂-NC, EG/CoS₂/CoS₂-NC, and Ir/C for OER, b) Overpotentials of EG/CoS₂, EG/CoS₂-NC, EG/CoS₂/CoS₂-NC, and Ir/C at current densities of 10 mA cm⁻² and 50 mA cm⁻², c) Tafel slopes of EG/CoS₂, EG/CoS₂-NC, EG/CoS₂/CoS₂-NC, and Ir/C, d) EIS plots of EG/CoS₂/CoS₂-NC, EG/CoS₂, and EG/CoS₂-NC for OER. e) Polarization curves of EG/CoS₂/CoS₂-NC before and after 1000 cycles without *iR*-correction. Inset: amperometric *i-t* curve of EG/CoS₂/CoS₂-NC. f) C_{dl} of EG/CoS₂, EG/CoS₂-NC, and EG/CoS₂/CoS₂-NC.

further compared (Figure 3b), and the overpotential of EG/CoS₂/CoS₂-NC is merely 311 mV. However, the overpotentials for all other electrodes are much higher than 311 mV at the same current density of 50 mA cm⁻² (e.g. 330 mV for EG/CoS₂, 426 mV for EG/CoS₂-NC, and 510 mV for commercial Ir/C), which further confirms the advantages of 3D EG/CoS₂/CoS₂-NC for promoting OER. More importantly, the OER catalytic activity of EG/CoS₂/CoS₂-NC is well comparable with that of the previously reported state-of-the-art CoS₂-based electrocatalysts (Table S1), for instance, CoS₂(400)/N,S-GO (380 mV at 10 mA cm⁻²),^[15] and A-CoS_{4.6}O_{0.6} (290 mV at 10 mA cm⁻²).^[14a]

The Tafel slope plot of a series of electrocatalysts was displayed in Figure 3c, in which the OER kinetics on different electrodes was reflected. It is notable that the Tafel slope of EG/CoS₂/CoS₂-NC is only 61.9 mV dec⁻¹, which is the smallest one among these catalysts (85.1 mV dec⁻¹ for EG/CoS₂, 98.7 mV dec⁻¹ for EG/CoS₂-NC, and 84.5 mV dec⁻¹ for commercial Ir/C). This result implies that the EG/CoS₂/CoS₂-NC could effectively catalyze OER by a more facile reaction process. The efficient charge transport property of the EG/CoS₂/CoS₂-NC hybrid was further confirmed by the electrochemical impedance spectroscopy (EIS). The EIS plots in Figure 3d reveal that the EG/CoS₂/CoS₂-NC exhibits the fastest charge transfer ability for OER, because the charge-transfer resistance of EG/CoS₂/CoS₂-NC was much smaller than that of EG/CoS₂ and EG/CoS₂-NC. The multi-current steps curve of EG/CoS₂/CoS₂-NC is shown in Figure S6. The initial and final current densities are 10 and 100 mA cm⁻², respectively, with an increase of 10 mA cm⁻² for each step. It is notable that the EG/CoS₂/CoS₂-NC works well under different potentials from low to high, and responds quickly to the change of potentials. These results indicate that the EG/CoS₂/CoS₂-NC could efficiently boost the charge transfer

process and mass transportation procedure. The catalytic stability of EG/CoS₂/CoS₂-NC was tested, and the result was displayed in Figure S7. A constant current density of 20 mA cm⁻² was exerted to this system. The initial potential is 1.51 V, and only an increase by 30 mV after a continuous reaction for 10 h is observed, demonstrating the high stability. Cyclic voltammetry was further applied to investigate the stability of EG/CoS₂/CoS₂-NC, and polarization curves in Figure 3e show that almost no decrease in catalytic activity appears even after 1000 cycles. The same conclusion could also be drawn from the inset amperometric *i-t* curve of EG/CoS₂/CoS₂-NC, where the current density remains 30.9 mA cm⁻² at 1.6 V for 10 h, indicating a robust durability of EG/CoS₂/CoS₂-NC electrode. Such an impressive stability may be attributed to the protection from the carbon shells^[17] during the OER procedure.

To understand the excellent OER performance of EG/CoS₂/CoS₂-NC, the electrochemically active surface area (ECSA) was estimated and compared by testing the electrochemical double layer capacitance (C_{dl}) with cyclic voltammetry (Figure 3f).^[18] As expected, the EG/CoS₂/CoS₂-NC hybrid has the largest C_{dl} value among EG/CoS₂/CoS₂-NC, EG/CoS₂, and EG/CoS₂-NC. The C_{dl} of EG/CoS₂/CoS₂-NC is 31.4 mF cm⁻², nearly 50% higher than that of EG/CoS₂ (23.4 mF cm⁻²), and three times higher than that of EG/CoS₂-NC (8.18 mF cm⁻²), respectively. Considering that a larger C_{dl} means a larger ECSA, the results show that the EG/CoS₂/CoS₂-NC possesses a considerable ECSA, which can substantially expedite the OER process.^[19]

In order to point out the active species of EG/CoS₂/CoS₂-NC in OER, in-situ Raman spectroscopy and ex-situ XRD measurement were employed. The in-situ Raman spectra of EG/CoS₂/CoS₂-NC are shown in Figure 4a, from which the Raman peaks from Co–O and Co–OOH bonds are observed, indicating the

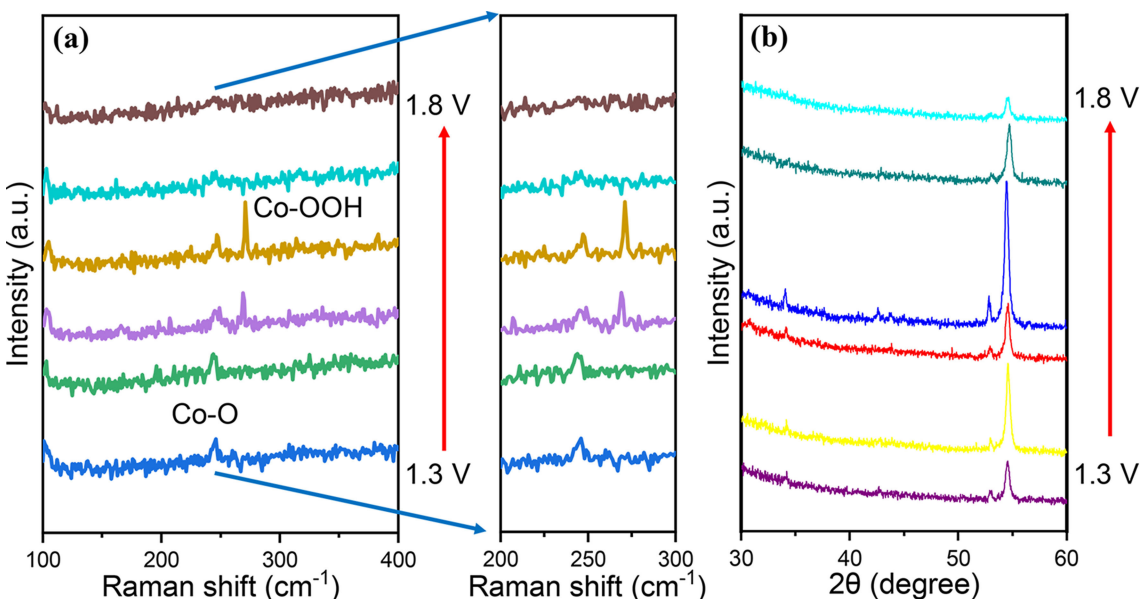


Figure 4. a) Potential-dependent in-situ Raman spectra of EG/CoS₂/CoS₂-NC during the OER, b) Potential-dependent ex-situ XRD patterns of EG/CoS₂/CoS₂-NC during the OER.

active species of EG/CoS₂/CoS₂-NC should be originated from Co–O and/or Co–OOH groups.^[20] Below 1.4 V, only Co–O bonds can be observed, however, when the potential was increased to 1.5 V, the Co–OOH bonds were further detected, revealing a transformation from Co–O to Co–OOH species during OER. The observed Co–O groups were generated from the oxidation of original Co–S groups in the EG/CoS₂/CoS₂-NC during the OER in alkaline electrolyte. The formed Co–O groups were further transformed to Co–OOH species with the increase of potential, in which the Co–OOH species could contribute to the superb catalytic performance.^[7b,21] This result is well consistent with the previously reported phenomenon that the Co–OOH would appear in high potential range during OER.^[16a, 22] It is also notable that beyond 1.7 V, the peak intensities of both Co–O and Co–OOH bonds were diminished. It is supposed that under such a high potential, the OER reaction was rather fast and the current density even could achieve 200 mA cm⁻² at 1.7 V (without *iR* correction), thus resulting in the fact that the active intermediates of Co–O groups and Co–OOH species were extremely hard to be detected under such high potentials. Corresponding XRD patterns of EG/CoS₂/CoS₂-NC confirmed that the CoO was generated during OER process (Figure 4b), while the CoO could be derived from Co–O and Co–OOH. Due to the exceptionally high catalytic activity of the Co–OOH species, the presented excellent performance towards OER could be explained.^[16a]

Besides the excellent OER catalytic performance, the EG/CoS₂/CoS₂-NC possesses superb activity to drive the oxidation reaction of other substances, such as urea and hydrazine. Thus, the electrochemical evaluation of urea oxidation and hydrazine oxidation reactions were conducted in 1.0 M KOH solution with additional 0.5 M urea or hydrazine^[23] via a typical three-electrode system. Figure 5a and Figure 5d show the polarization curves for electrochemical urea oxidation and hydrazine

oxidation reactions, respectively. It could be noticed that at a potential of 1.5 V, the current density of EG/CoS₂/CoS₂-NC achieves 35.5 mA cm⁻² for urea oxidation reaction, which is nearly twice times than that of the sum of EG/CoS₂ (11.2 mA cm⁻²) and EG/CoS₂-NC (7.0 mA cm⁻²), which indicates that the synergistic effect between CoS₂ and CoS₂-NC could exceptionally enhance the catalytic performance towards urea oxidation reaction. Such a synergy could be further reflected by the electrochemical hydrazine oxidation reaction, where the current density of EG/CoS₂/CoS₂-NC reaches 53.6 mA cm⁻² at 0.6 V, higher than the sum of EG/CoS₂ (31.2 mA cm⁻²) and EG/CoS₂-NC (2.5 mA cm⁻²). It could be also concluded from the Tafel slope plot in Figure 5b and Figure 5e that the EG/CoS₂/CoS₂-NC displays a wonderful ability to drive two oxidation reactions easily because the Tafel slopes of EG/CoS₂/CoS₂-NC (262 mV dec⁻¹ for urea oxidation reaction and 89.7 mV dec⁻¹ for hydrazine oxidation reaction) are much smaller than that of EG/CoS₂-NC (309 mV dec⁻¹ for urea oxidation reaction and 154 mV dec⁻¹ for hydrazine oxidation reaction) and EG/CoS₂ (267 mV dec⁻¹ for urea oxidation reaction and 121 mV dec⁻¹ for hydrazine oxidation reaction).

The multi-current chronopotentiometric curves were further utilized to investigate the mechanical property of EG/CoS₂/CoS₂-NC (Figure 5c and Figure 5f). The current density increases from 10 to 100 mA cm⁻² for urea oxidation reaction and 20 to 70 mA cm⁻² for hydrazine oxidation reaction. The increase of current density for each step is 10 mA cm⁻², and the resulting consequence could be obtained. It is observed that the potential could quickly respond the altering of current density within 500 s,

which proclaims the remarkable mechanical robustness property of EG/CoS₂/CoS₂-NC. The stability tests for both oxidation reactions were conducted and displayed in Figure S8, where the chronopotentiometric method was applied with a

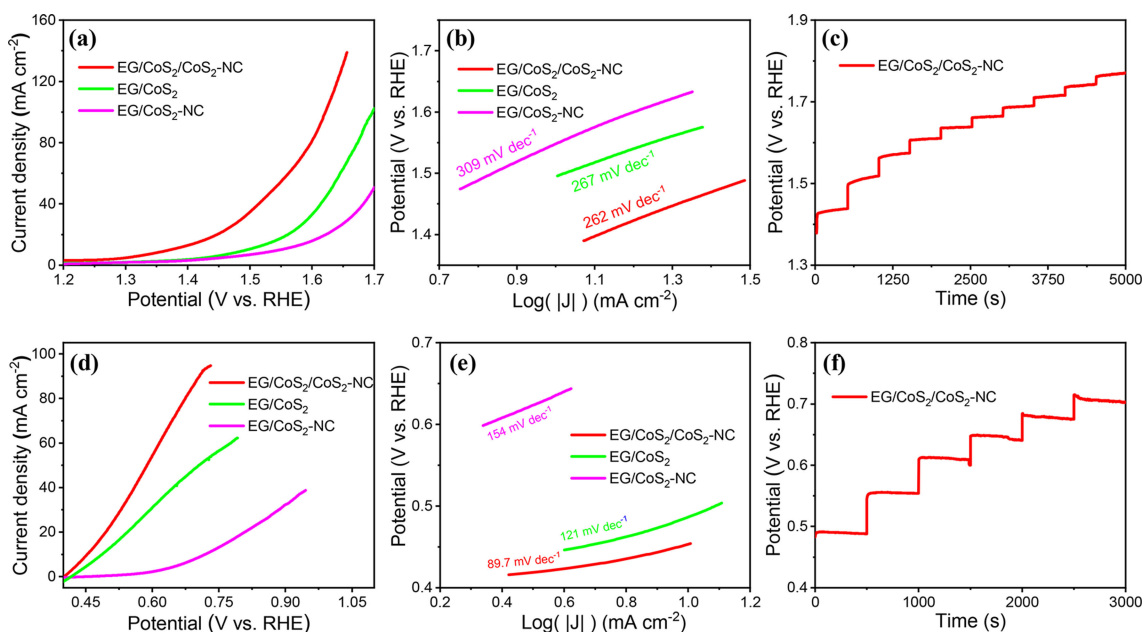


Figure 5. a) Polarization curves of EG/CoS₂, EG/CoS₂-NC, and EG/CoS₂/CoS₂-NC for urea oxidation, b) Tafel slopes of EG/CoS₂, EG/CoS₂-NC, and EG/CoS₂/CoS₂-NC for urea oxidation, c) multi-current steps curve of EG/CoS₂/CoS₂-NC for urea oxidation, d) polarization curves of EG/CoS₂, EG/CoS₂-NC, and EG/CoS₂/CoS₂-NC for hydrazine oxidation, e) Tafel slopes of EG/CoS₂, EG/CoS₂-NC, and EG/CoS₂/CoS₂-NC for hydrazine oxidation, f) multi-current steps curve of EG/CoS₂/CoS₂-NC for hydrazine oxidation.

current density of 20 mA cm⁻². The remarkable durability of EG/CoS₂/CoS₂-NC is further evidenced by the almost zero-change in voltage for both urea oxidation reaction (1.62 V) and hydrazine oxidation reactions (0.51 V) after a long-term test of 10 h.

In conclusion, a novel 3D EG/CoS₂/CoS₂-NC hybrid electrocatalyst with core-shell structure was developed by the sulfurization treatment of EG-supported Co(OH)₂/ZIF-67 precursor. The 10-nm thick outer shell is composed of CoS₂ embedded into the N-doped carbon derived from the ZIF-67, while the CoS₂ core has a particle size of ~20 nm as a result of the sulfurized Co(OH)₂ nanosheets array. The as-prepared EG/CoS₂/CoS₂-NC hybrid delivered an excellent electrocatalytic performance for OER with a low overpotential of 210 mV at 10 mA cm⁻², and a small Tafel slope of 61.9 mV dec⁻¹, which is far superior to that of Ir/C, and higher than those of other reported state-of-the-art CoS₂-based electrocatalysts. Such an excellent activity is mainly attributed from the synergistic effect and unique 3D core-shell structure. The highly active catalytic sites of Co-OOH species derived from Co-S groups during OER could be identified by the in-situ Raman spectroscopy and ex-situ XRD pattern. Further, the EG/CoS₂/CoS₂-NC hybrid could boost urea and hydrazine oxidation reactions with impressive stability. It is also believed that the EG/CoS₂/CoS₂-NC hybrid in the present work would inspire the rational design towards 3D electrocatalysts composed of transition metal sulfides/transition metal sulfides embedded into N-doped carbon shells, which may stand out in various electrochemical applications, such as supercapacitors, solar cells, and fuel cells.

Acknowledgements

Y. Hou thanks the support of NSFC 51702284 and 21878270, Fundamental Research Funds for the Central Universities (112109*172210171) and the Startup Foundation for Hundred-Talent Program of Zhejiang University (112100-193820101/001/022).

Conflict of Interest

The authors declare no conflict of interest.

Keywords: active sites · cobalt dichalcogenides · core-shell structures · nitrogen-doped carbon · oxygen evolution reaction

- [1] a) C. Lei, Y. Wang, Y. Hou, P. Liu, J. Yang, T. Zhang, X. Zhuang, M. Chen, B. Yang, L. Lei, C. Yuan, M. Qiu, X. Feng, *Energy Environ. Sci.* **2018**, DOI: 10.1039/c8ee01841c; b) C. Lei, H. Chen, J. Cao, J. Yang, M. Qiu, Y. Xia, C. Yuan, B. Yang, Z. Li, X. Zhang, L. Lei, J. Abbott, Y. Zhong, X. Xia, G. Wu, Q. He, Y. Hou, *Adv. Energy Mater.* **2018**, 1801912; c) D. Geng, N. Ding, T. S. A. Hor, S. W. Chien, Z. Liu, D. Wuu, X. Sun, Y. Zong, *Adv. Energy Mater.* **2016**, 6, 1502164; d) J. Mei, T. Liao, L. Kou, Z. Sun, *Adv. Mater.* **2017**, 29, 1700176; e) C. Sun, Q. Xu, Y. Xie, Y. Ling, Y. Hou, *J. Mater. Chem. A* **2018**, 6, 8289–8298; f) D. Yan, C. Dong, Y. Huang, Y. Zou, C. Xie, Y. Wang, Y. Zhang, D. Liu, S. Shen, S. Wang, *J. Mater. Chem. A* **2018**, 6, 805–810.
- [2] a) S. Zhao, Y. Wang, J. Dong, C. T. He, H. Yin, P. An, K. Zhao, X. Zhang, C. Gao, L. Zhang, J. Lv, J. Wang, J. Zhang, A. M. Khattak, N. A. Khan, Z. Wei, J. Zhang, S. Liu, H. Zhao, Z. Tang, *Nat. Energy* **2016**, 1, 16184; b) X. R. Wang, J. Y. Liu, Z. W. Liu, W. C. Wang, J. Luo, X. P. Han, X. W. Du, S. Z. Qiao, J. Yang, *Adv. Mater.* **2018**, 30, 1800005; c) Y. Wang, M. Qiao, Y. Li, S. Wang, *Small* **2018**, 14, e1800136; d) X. Cheng, C. Lei, J. Yang, B. Yang, Z.

- Li, J. Lu, X. Zhang, L. Lei, Y. Hou, K. K. Ostrikov, *ChemElectroChem* **2018**, DOI: 10.1002/celc.201801104.
- [3] Y. Hou, M. Qiu, T. Zhang, X. Zhuang, C. S. Kim, C. Yuan, X. Feng, *Adv. Mater.* **2017**, *29*, 1604480.
- [4] H. Cheng, M. L. Li, C. Y. Su, N. Li, Z. Q. Liu, *Adv. Funct. Mater.* **2017**, *27*, 1701833.
- [5] Y. Q. Zhang, M. Li, B. Hua, Y. Wang, Y. F. Sun, J. L. Luo, *Appl. Catal. B: Environ.* **2018**, *236*, 413–419.
- [6] a) Y. Hou, X. Zhuang, X. Feng, *Small Methods* **2017**, *1*, 1700090; b) L. Huang, R. Chen, C. Xie, C. Chen, Y. Wang, Y. Zeng, D. Chen, S. Wang, *Nanoscale* **2018**, *10*, 13638–13644; c) D. Liu, L. Tao, D. Yan, Y. Zou, S. Wang, *ChemElectroChem* **2018**, *5*, 1775–1785.
- [7] a) S. Peng, L. Li, X. Han, W. Sun, M. Srinivasan, S. G. Mhaisalkar, F. Cheng, Q. Yan, J. Chen, S. Ramakrishna, *Angew. Chem. Int. Ed.* **2014**, *53*, 12594–12599; *Angew. Chem.* **2014**, *126*, 12802–12807; b) C. Guan, X. Liu, A. M. Elshahawy, H. Zhang, H. Wu, S. J. Pennycook, J. Wang, *Nanoscale Horiz.* **2017**, *2*, 342–348; c) W. Niu, Z. Li, K. Marcus, L. Zhou, Y. Li, R. Ye, K. Liang, Y. Yang, *Adv. Energy Mater.* **2018**, *8*, 1701642.
- [8] a) S. Gadielli, T. Zhao, S. A. Shevlin, Z. Guo, *Energy Environ. Sci.* **2016**, *9*, 1661–1667; b) T. Zhang, Y. Hou, V. Dzhagan, Z. Liao, G. Chai, M. Loffler, D. Olianas, A. Milani, S. Xu, M. Tommasini, D. R. T. Zahn, Z. Zheng, E. Zschech, R. Jordan, X. Feng, *Nat. Commun.* **2018**, *9*, 1140.
- [9] a) M. Zhang, Q. Dai, H. Zheng, M. Chen, L. Dai, *Adv. Mater.* **2018**, *30*, 10; b) S. Chen, J. Duan, M. Jaroniec, S. Z. Qiao, *Adv. Mater.* **2014**, *26*, 2925–2930.
- [10] R. Ghosh Chaudhuri, S. Paria, *Chem. Rev.* **2012**, *112*, 2373–2433.
- [11] a) Y. Guo, J. Tang, H. Qian, Z. Wang, Y. Yamauchi, *Chem. Mater.* **2017**, *29*, 5566–5573; b) Y. Pan, K. Sun, S. Liu, X. Cao, K. Wu, W. C. Cheong, Z. Chen, Y. Wang, Y. Li, Y. Liu, D. Wang, Q. Peng, C. Chen, Y. Li, *J. Am. Chem. Soc.* **2018**, *140*, 2610–2618.
- [12] J. Hao, W. Yang, Z. Peng, C. Zhang, Z. Huang, W. Shi, *ACS Catal.* **2017**, *7*, 4214–4220.
- [13] J. Xie, S. Liu, G. Cao, T. Zhu, X. Zhao, *Nano Energy* **2013**, *2*, 49–56.
- [14] a) P. Cai, J. Huang, J. Chen, Z. Wen, *Angew. Chem. Int. Ed.* **2017**, *56*, 4858–4861; *Angew. Chem.* **2017**, *129*, 4936–4939; b) H. Li, Y. Gao, Y. Shao, Y. Su, X. Wang, *Nano Lett.* **2015**, *15*, 6689–6695.
- [15] P. Ganesan, M. Prabu, J. Sanetuntikul, S. Shanmugam, *ACS Catal.* **2015**, *5*, 3625–3637.
- [16] a) H. Han, K. M. Kim, H. Choi, G. Ali, K. Y. Chung, Y. R. Hong, J. Choi, J. Kwon, S. W. Lee, J. W. Lee, J. H. Ryu, T. Song, S. Mhin, *ACS Catal.* **2018**, *8*, 4091–4102; b) B. Weng, C. R. Grice, W. Meng, L. Guan, F. Xu, Y. Yu, C. Wang, D. Zhao, Y. Yan, *ACS Energy Lett.* **2018**, 1434–1442.
- [17] D. Zhao, Y. Pi, Q. Shao, Y. Feng, Y. Zhang, X. Huang, *ACS Nano* **2018**, *12*, 6245–6251.
- [18] Y. Yang, L. Dang, M. J. Shearer, H. Sheng, W. Li, J. Chen, P. Xiao, Y. Zhang, R. J. Hamers, S. Jin, *Adv. Energy Mater.* **2018**, *8*, 1703189.
- [19] a) J. Z. Liu, Y. F. Ji, J. W. Nai, X. G. Niu, Y. Luo, L. Guo, S. H. Yang, *Energy Environ. Sci.* **2018**, *11*, 1736–1741; b) Y. Y. Ma, Z. L. Lang, L. K. Yan, Y. H. Wang, H. Tan, K. Feng, Y. Xia, J. Zhong, Y. Liu, Z. Kang, Y. G. Li, *Energy Environ. Sci.* **2018**, *11*, 2114–2123; c) J. Cao, C. Lei, J. Yang, X. Cheng, Z. Li, B. Yang, X. Zhang, L. Lei, Y. Hou, K. Ostrikov, *J. Mater. Chem. A* **2018**, *6*, 18877–18883.
- [20] a) M. R. Liu, Q. L. Hong, Q. H. Li, Y. H. Du, H. X. Zhang, S. M. Chen, T. H. Zhou, J. Zhang, *Adv. Funct. Mater.* **2018**, *28*, 1801136; b) J. Huang, J. Chen, T. Yao, J. He, S. Jiang, Z. Sun, Q. Liu, W. Cheng, F. Hu, Y. Jiang, Z. Pan, S. Wei, *Angew. Chem. Int. Ed.* **2015**, *54*, 8722–8727; *Angew. Chem.* **2015**, *127*, 8846–8851; c) P. Chen, K. Xu, Z. Fang, Y. Tong, J. Wu, X. Lu, X. Peng, H. Ding, C. Wu, Y. Xie, *Angew. Chem. Int. Ed.* **2015**, *54*, 14710–14714; *Angew. Chem.* **2015**, *127*, 14923–14927.
- [21] S. Jin, *ACS Energy Lett.* **2017**, *2*, 1937–1938.
- [22] V. Vij, S. Sultan, A. M. Harzandi, A. Meena, J. N. Tiwari, W. G. Lee, T. Yoon, K. S. Kim, *ACS Catal.* **2017**, *7*, 7196–7225.
- [23] Q. He, Y. Wan, H. Jiang, Z. Pan, C. Wu, M. Wang, X. Wu, B. Ye, P. M. Ajayan, L. Song, *ACS Energy Lett.* **2018**, *3*, 1373–1380.

Manuscript received: October 1, 2018

Accepted Article published: October 16, 2018

Version of record online: October 31, 2018